Optimization of Multi Element Rear Wing

– Optimization of angles and positioning for maximum down-force using Computational Fluid Dynamics

**Erik Nygårds, eriny141**
Shreyas Maligemane, shrma734

Contents

1 Introduction

Racing cars are in a constant engineering battle to become faster and faster. There are many ways to decrease the lap times of a racecar, such as engine development, chassis improvement, or improvements to the aerodynamics of the vehicle. The main goal of aerodynamic development of a racecar is to increase negative lift, in other words increase downforce, and decrease drag. The weighting of these opposing goals depend heavily on the vehicle and the track where it will go competing. A track with long straights and few corners will, for example, favour vehicles with low drag. While a slower twistier course will favour those with high downforce. Many racecars feature a multi element rear wing, which produces large amounts of downforce. The multi element rear wings consist of two or more aerofoil-shaped elements, which are positioned in such a way that they help each other to generate more negative lift than a single element rear wing would. However, finding the optimal positions and angles is not an easy task. Though this can be done using Computational Fluid Dynamics (CFD), for a relatively low cost compared to wind tunnel tests, with sufficient accuracy.

In this report the performance of a two-element rear wing was optimized for maximum downforce. The airfoil for both elements were the NACA-6315. The CFD simulations were made using the RANS Spalart-Allmaras turbulence model. The model was optimized by varying the angle of attack (AoA) of both airfoils as well as the position of the second element.

A common way to increase downforce from a wing is to add a flap to the trailing edge, a so-called Gurney flap. To study the effects of this, and to investigate methods for design space filling, a Gurney flap was added to the previously optimised arrangement of the wing elements. The flap was optimised for downforce generation and its effect on the flow was investigated.
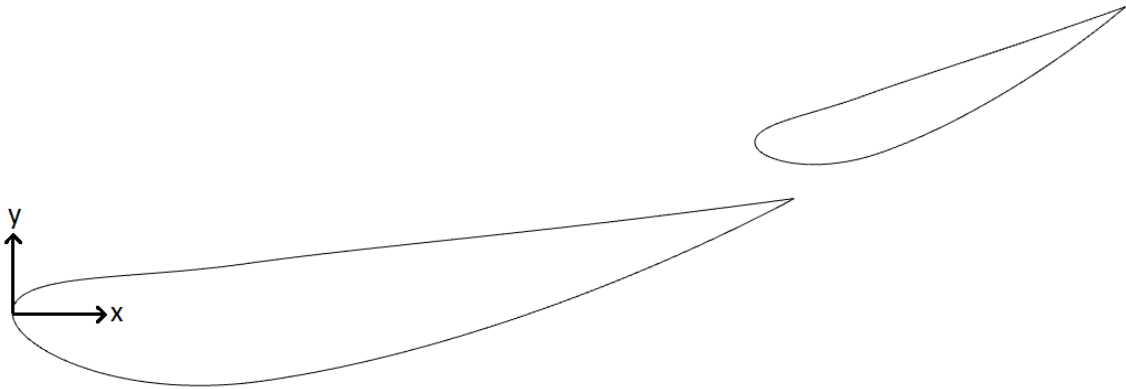

Figure 1: Two element rear wing using the NACA-6315 airfoil, arrangement used for mesh verification.

2   Method

In this section the method used will be presented, including mesh verification and validation.

2.1   Model

The data points of the airfoil imported from AirfoilTools [1] were scaled down to 0.4[m] and 0.2[m] chord length for the first and second element respectively. The airfoil used for both elements was the NACA-6315. A 2-D surface was created after flipping the airfoils to generate negative lift (downforce). The geometries were positioned with specific constraints for parametric study. The constraints ensure to limit the meshing issues and obtain reliable results from RANS modelling. A C-grid, tetrahedral dominant unstructured mesh was created, this can be seen in figure 2. The walls were 8 chord lengths away from the airfoil in all directions, to ensure the boundary walls did not influence the flow. Body of influence was used to enhance the intensity of mesh around the airfoil. To capture boundary layer $y^+ \sim 1$ was achieved with inflation layers on the no-slip walls (airfoils).
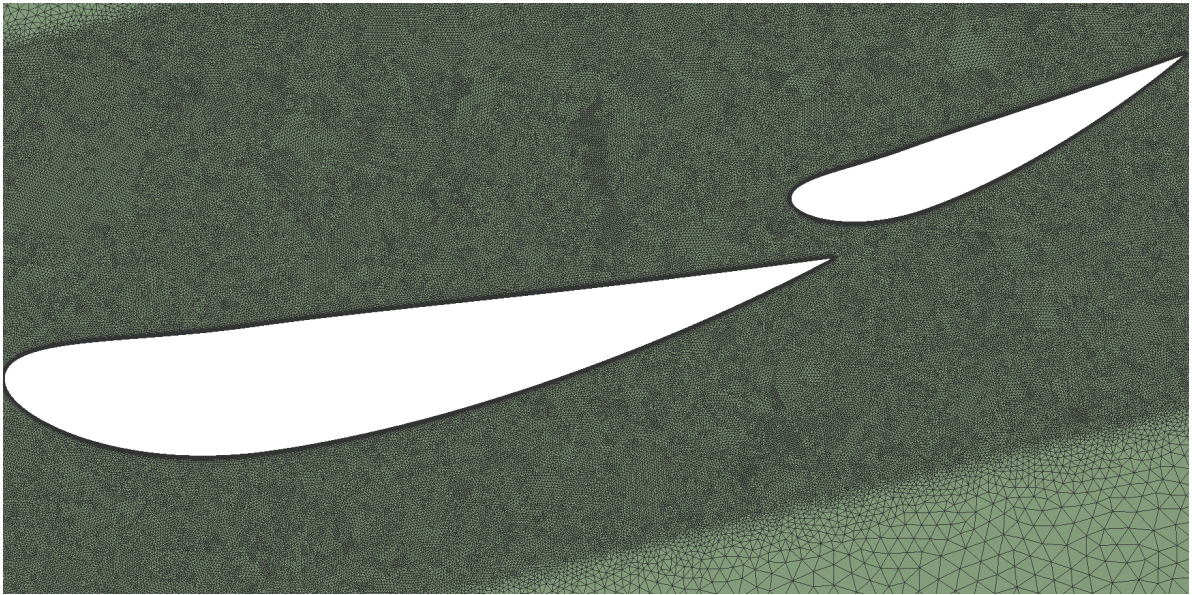
Figure 2: The unstructured medium mesh used.

As mentioned previously, the model was constructed using parameters to vary the angles of the two elements, and the position of the second element. The angle of attack (AoA) of the two elements were simply defined as the angle between a horizontal line and the chord line. The y-position of the second airfoil was defined as a percentage of the chord length of the first element, plus a correction height based on the angle of the first element, see equation 1. Where the correction height ensures the second airfoil does not coincide with the first element when its AoA increases.

$$y = y_{\text{pos}} C_{\text{element},1} + y_{\text{pos}} C_{\text{element},1} \sin \alpha_{\text{element},1} \tag{1}$$

Where α is the angle of attack, and y_{pos} a percentage value of the first elements chord length. Similarly the x-position was defined as a percentage of the first elements chord length, see equation 2.

$$x = x_{\text{pos}} C_{\text{element},1} \tag{2}$$

2

The chord lengths for the two elements, above $C_{element,1}$ and $C_{element,2}$, will be referred to as C_1 and C_2 respectively from this point onward. All position values henceforth is presented as the percentage chord values, e.g. y_{pos} and x_{pos}.

2.2 Boundary Condition and Solver setup

Spalart Allmaras turbulence model was chosen as it has been proven to provide accurate results for airfoils [2]. The inlet velocity was set to 19.44[m/s], corresponding to 70 km/h, and a pressure outlet with zero gauge pressure for the outlet. No-slip walls were used on the airfoils, with symmetry used on the horizontal top and bottom wall. The solver setup used for the study can be seen in table 1. The coefficients of lift and drag (C_L, C_D) were reported as output parameters for the design optimization.

Table 1: The solution methods opted for the study

Solution method	Opted methods
Pressure-Velocity coupling	Coupled
Spatial Discretization	
Gradient	Least square method
Pressure	Standard
Momentum, TKE, Specific dissipation rate, Modified Turbulent Viscosity	Second Order Upwind

2.3 Verification

A mesh verification was made to attain mesh independence as per Celik et al.[3]. The parameters chosen were total coefficient of lift and drag. An acceptable limit of 3% deviation between the meshes was considered. This criterion was achieved between the fine and medium mesh, see table 3. Hence, medium mesh was considered for all the simulations and design study. The mesh verification was performed using the geometry settings presented in table 2.

Table 2: The parameter values used for the mesh verification.

Parameter	Value
Element 1 AoA [°]	8
Element 2 AoA [°]	20
Element 2 y-position [-]	0.94
Element 2 x-position [-]	0.08

Table 3: Result of the mesh verification using the geometrical parameters specified in table 2. All values in percentage.

	elements			e_a^{32}	e_{ext}^{32}	GCI^{32}	e_a^{21}	e_{ext}^{21}	GCI^{21}
N1	747622	r21=1.37	C_L	0.23	0.29	0.37	0.13	0.16	0.2
N2	399944		C_D	3.82	0.45	0.56	0.41	0.04	0.05
N3	221672	r23=1.34							

2.4 Design Optimization

The rear wing design was optimized using Ansys Workbench built in 'Design of Experiments'. Design points were generated using Optimal Space Filling (OSF), and face centered Central-Composite Design (CCD) to capture the extreme design points. Latin-Hypercube Sampling (LHS) was used to generate extra data points, as well as 10 verification points. The angles and the positioning of the 2nd element was used as input parameters, while C_L and C_D was used as output parameters. The input parameters were constrained with min- and max-values based on a few initial simulations, as well as mesh constraints. The found limits can be seen in table 4. The gap between the two airfoils was particularly constrained by the mesh, as the inflation layers interacted if they were too close at certain angles. However, this was not an issue with the limits in table 4.

Table 4: The limits used for the parameters in the optimisation.

Min	Parameter	Max
8°	Element 1 AoA	15°
25°	Element 2 AoA	35°
0.073 [-]	y-position	0.2 [-]
0.8 [-]	x-position	1.2 [-]

A response surface was generated using the design points generated by the different point generating methods specified earlier. The accuracy and strengths of the response surface generating methods was investigated by comparing the errors to both verification and learning points. The most accurate response surface was then used to find an optimal point using the Multi-objective Genetic Algorithm (MOGA), as it is good at finding global optimum. As opposed to methods such as Non-Linear Programming by Quadratic Lagrangian (NLPQL) which risk falling into local optimum.[4]

2.5 Device improvement

To improve the downforce of the rear wing a Gurney flap was added to the trailing edge of the second element, see figure 3. The flap was optimised with regards to flap height and angle for maximum downforce, or minimum C_L. Due to the design space being simple, only consisting of two variables, the way the design space exploration algorithms fill the design space was investigated. It was then simple to see the strengths and weaknesses of the algorithms.
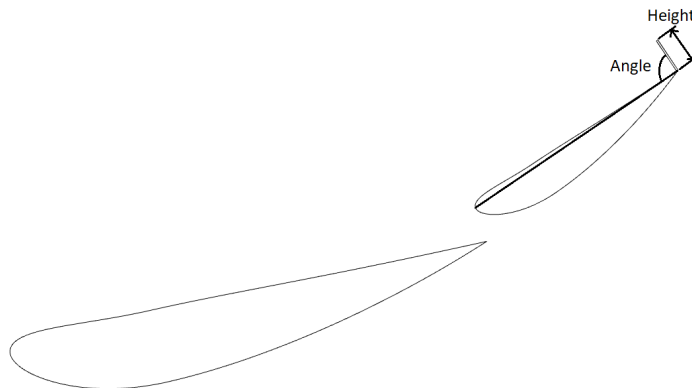
Figure 3: The geometry and element arrangement used for the flap investigation.

Limits of the flaps two parameters were set somewhat arbitrary, only based on the fact that flaps

are used when the element size cannot be increased. Thus, it should not extend further rearward than the element itself. The limits can be seen in table 5.

Table 5: The limits used for the flap optimisation, where the height is normalised with the second element chord length C_2.

Min	Parameter	Max
60°	Angle	120°
0.025 [-]	Height	0.15 [-]

The found optimal arrangement for the flap was used to investigate the impact the flap has on the flow. As well as how the parameters impact the result, in terms of sensitivity and performance.

3 Results

In this section the results from the optimisations will be presented.

3.1 Element Arrangement Optimisation

The results of the investigation of the response surface generation methods can be seen in table 6.

Table 6: The error percentages of the different response surface generating methods to verification and learning points. Where RMSE is the Root Mean Square Error, and RMAE the Relative Maximum Absolute Error.

	Genetic Aggregation	Kriging	Non-Parametric Regression	Neural Network
To Verification Points				
CD - RMSE [%]	0.075	0.066	0.18	0.24
CL - RMSE [%]	1.24	0.42	0.81	5.74
CD - RMAE [%]	7.71	7.07	18.15	20.95
CL - RMAE [%]	11.75	5.34	4.38	49.49
To Learning Points				
CD - RMSE [%]	0.15	$\sim$0	0.35	0.76
CL - RMSE [%]	0.94	$\sim$0	1.34	10.59
CD - RMAE [%]	36.72	0	114.59	118.68
CL - RMAE [%]	18.51	0	44.80	123.18

The optimised arrangement settings, and the resulting lift and drag can be seen in table 7.

Table 7: Arrangement and resulting drag- and lift-coefficients for the optimised rear wing. Where α_1 and α_2 are the element 1 and element 2 AoA respectively.

	α_1	α_2	x-pos	y-pos		C_D	C_L
Value	12.773	33.899	0.952	0.081		0.0720	-1.7072

The configuration and its impact on the flow can be seen in figure 4.

Figure 4 clearly shows how the gap between the airfoils let higher velocity air in to the boundary layer on the underside of the top airfoil. Thus energising the boundary layer, keeping it attached to the second element. The impact of variations of the angles and positions, where unvaried parameters are the same as the optimised arrangement, can be seen in figures 5 and 6.

It can be seen that the AoA of the second element highly influences the downforce generated by the wing. For lower 2nd element angles, the angle of the first element becomes less sensitive
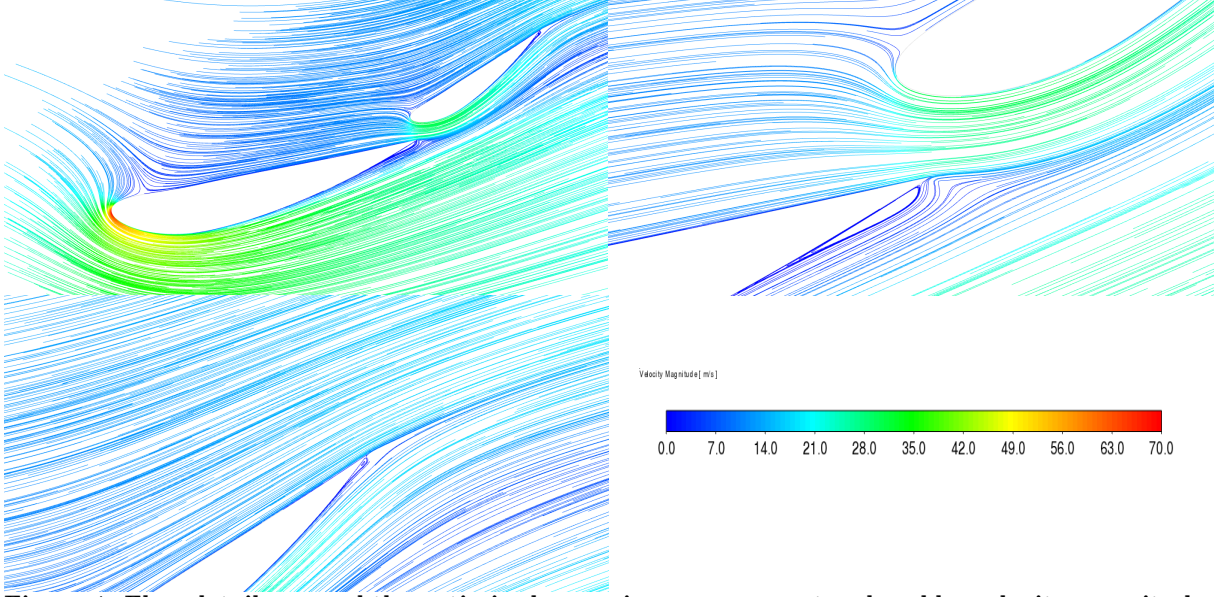
Figure 4: Flow details around the optimised rear wing arrangement, colored by velocity magnitude.
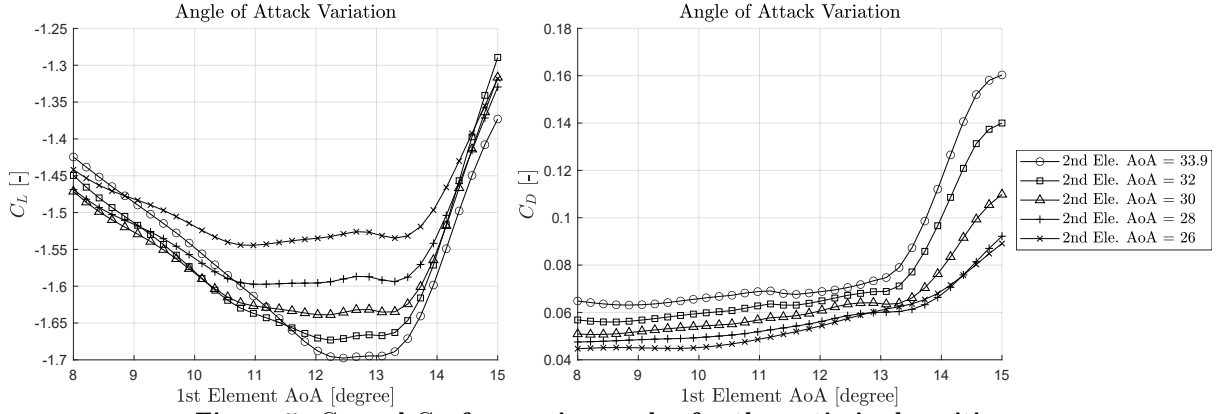

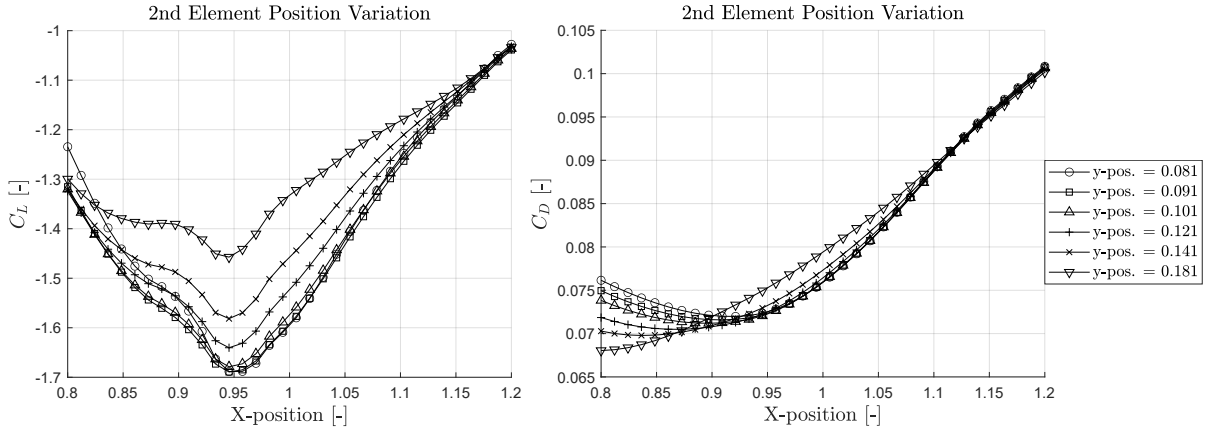**Figure 5: C_L and C_D for varying angles for the optimised position.**

Figure 6: C_L and C_D for varying positions for the optimised angles.

to changes, see figure 5. At high first element angles the rear wing rapidly loses downforce, while increasing drag significantly, for all second element angles. Figure 6 shows that for low y-positions there is little difference with small variations in C_L, while the sensitivity increases as the y-position increases. There is also a clear optimum range for maximum downforce, i.e. minimum C_L, for the x-position. Which seems to be similar for all y-positions. However, the drag does not show significant differences for different y-positions, while the drag increases with increasing x-position. Though it can be seen that drag is decreased more for the high mounted, far forward second element placements, see figure 6. The sensitivity of the different parameters can be represented as relative sensitivities, see figure 7.
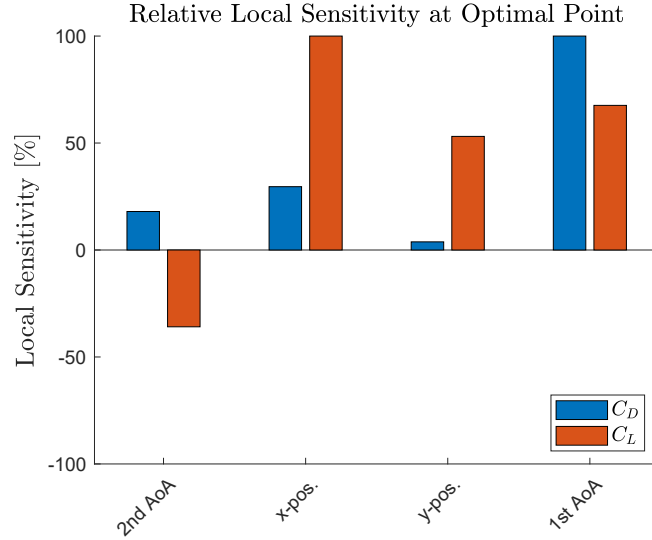
Figure 7: Relative sensitivities of the input parameters influence on the C_L and C_D at the optimised arrangement.

Figure 7 clearly shows that the x-position is the most sensitive parameter for the downforce. While the 1st element AoA is the most influential for the drag, with the other parameters sensitivity being low. The 2nd element AoA sensitivity indicate that a higher angle of attack decreases the C_L, i.e. increases downforce.

3.2 Device Improvement

The result of the design space exploration can be seen in figure 8.
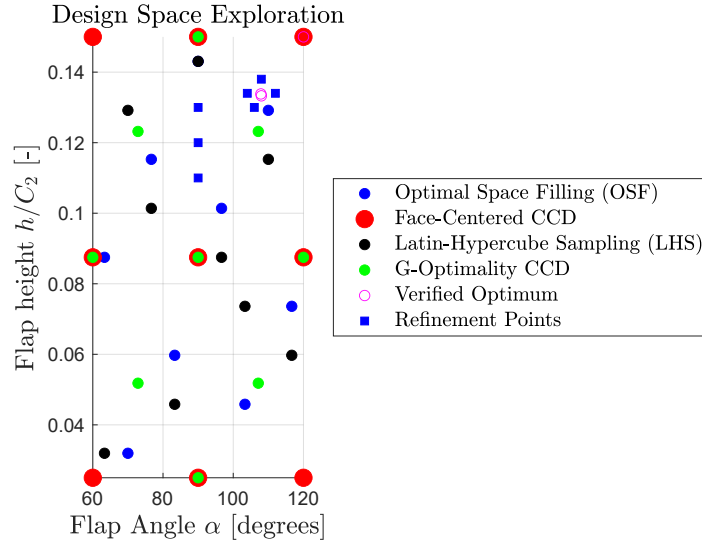
Figure 8: Design points generated, and added, for simulation. Where the area represents the design space.

The response surface generated by the design points from the design space exploration using the Kriging algorithm can be seen in figure 9.

The response surface clearly show large instabilities, in the form of sharp peaks and valleys, for large flap heights and angles above $\sim 90°$. It can also be seen that generally, the flap height influences the C_L the most, while for varying angles there are only small differences. The
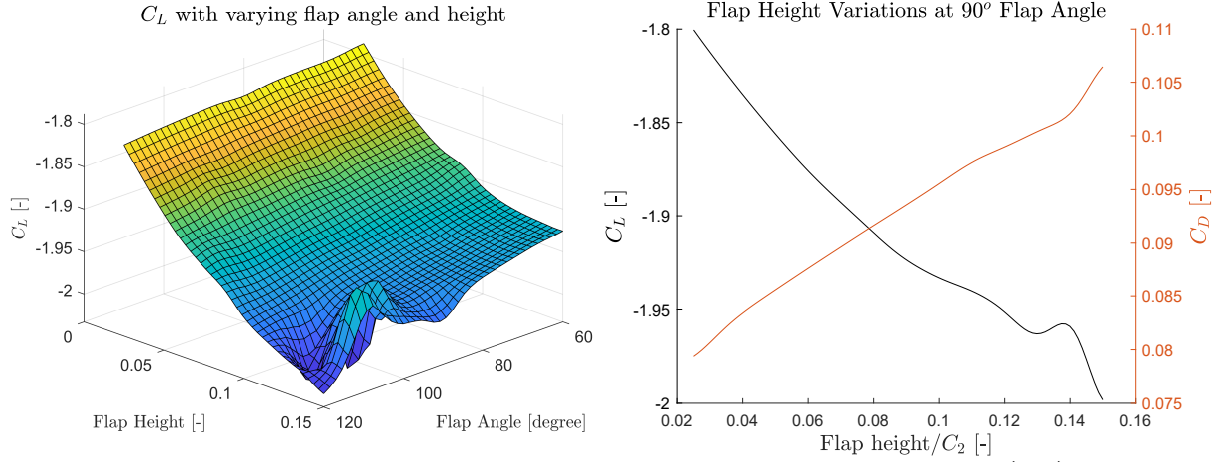
Figure 9: The response surface generated by using Kriging from the design points (left). Variations in C_L and C_D for varying flap heights at a flap angle of 90° (right).

variations of lift and drag for varying flap heights at a flap angle of 90° can be seen in figure 9 (right). Even at 90° flap angle some instabilities emerge for large flap heights, while there however is a clear trend of increased flap heights yielding more downforce with more drag. The impact of the Gurney flap on the flow can be seen in figure 10.
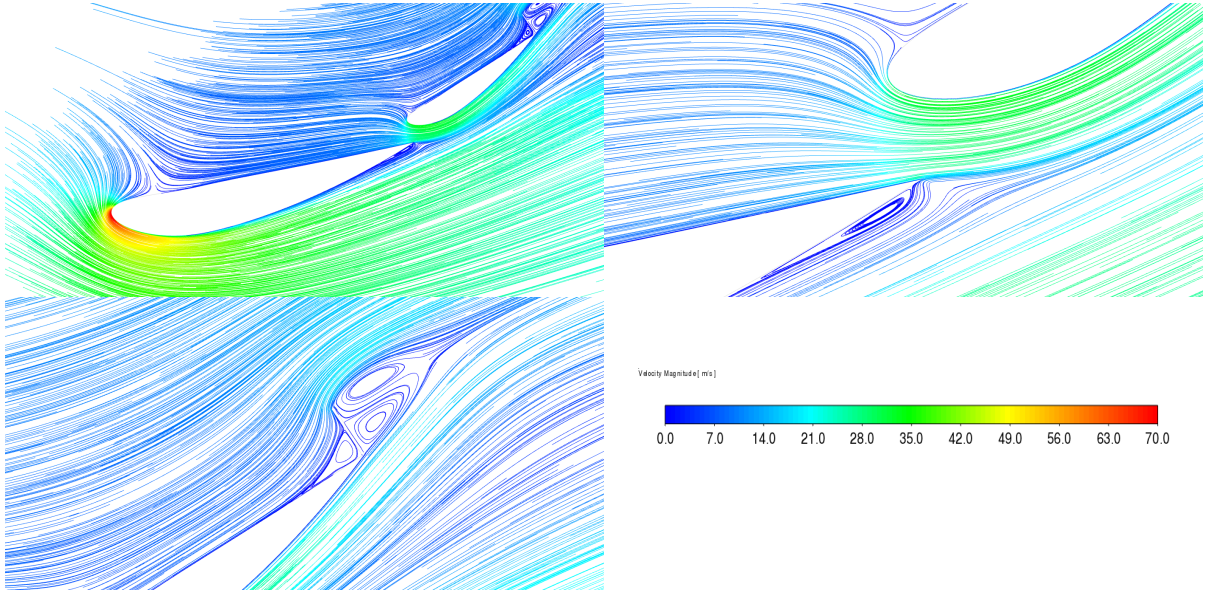
Figure 10: Flow details around the Gurney flap geometry, using a flap angle of 90°and a height of 0.15 h/C_2.

It can be seen that the recirculation behind the flap keeps the air attached to the airfoil longer, and also prevents it from aligning with the free stream velocity. Thus, sending more air upward, increasing downforce.

The performance of the flap using a flap height of 0.15 h/C_2 and a flap angle of 90° was a $C_L = -1.998$ and a $C_D = 0.106$. Giving a downforce increase of 17% compared to without a flap, and a drag increase of 47%.

4   Discussion

In this section the results and methods will be discussed.

4.1   Method

The limits set for the parameters were found by performing a preliminary optimisation, which indicated the angles had to be quite high, higher than first anticipated. Initially the parameters were based on found stall angles, around 12-15° for the NACA-6315 [2] [5]. However, due to the interference of the two airfoils, the separation was delayed, thus higher angles could be used, especially for the second airfoil element. As it can be seen in figure 7 an increase of the second element angle predicts an increase in downforce, indicating higher angles should be better. However, as higher angles lead to more separation, and unstable flow, which RANS models cannot capture, the angle was not increased further. The RANS model used is especially limiting when adding the Gurney flap, as the flow behind a Gurney flap is inherently unstable, producing a von Kármán vortex street [6]. As the flap height increases these unsteady effects increase as well. Which eventually manifests itself as chaotic results, see figure 9, where a small change to height or angle produces wildly different results. A remedy to this would be to use an unsteady solver, such as URANS, which is capable of capturing the unsteadiness more accurately. However, in the interest of time this was not done.

4.2   Arrangement Optimisation

The results show that the two airfoils can, when positioned and angled correctly, produce far more downforce than a single, larger airfoil could. This is due to the gap between the airfoils allowing higher velocity and energy air to enter the boundary layer. This energises the boundary layer, allowing it to stay attached for longer. The extra suction from the second element also helps the airflow stay attached on the trailing edge of the first element, see figure 4. In terms of the downforce generation, it can be seen in figure 6 that the x-position has a significant impact. This is because it influences where the energised boundary layer starts. If it starts too early, a low pressure region forms on top of the trailing region of the first element, thus reducing lift. If it starts too late the second airfoil would start increasing separation on the first element. Thus the x-position is important to get right, alongside the angles. However the x-position is the most sensitive parameter, as shown in figure 7.

The response surface generating methods investigation, see table 6, showed that Kriging provided the lowest errors to verification points, and was thus used. By definition it also provided the lowest errors to learning points. Non-Parametric and Neural Network both provided large errors, which could be due to the fact that they are good for noisy results [4]. Whereas the results from the design points proved to not be noisy, as the limits of the model were set within the working range of the Spalart-Allmaras model. Since the response was not noisy, the Kriging model fared well and gave good results. The genetic aggregation model was not far behind and was comparatively similar to the Kriging response surface. An advantage of using Kriging is that if the response becomes noisy when it should not, as it did for the device improvement, see figure 9, it is easy to spot. Allowing the user to identify the area where something is going wrong, which in this case was the flap creating too unsteady flows for the RANS-model to accurately predict.

4.3   Device Improvement

The design space visualisation, see figure 8, shows that multiple methods in combination are needed to explore the entire design space. While OSF is good at filling the 'interior' of the design space, it does not capture the extremes. In this case, it even left a large area in the 'top-

left' corner unexplored. A good combination is thus OSF with some kind of CCD, in this case Face-Centered and G-Optimality was visualised. As both capture extremes, although only Face-Centered captures the 'extreme-extreme', while G-Optimality only captures 'extreme-middle' points. Adding the LHS method points further increases the internal design space filling, which was necessary, as OSF alone does not provide enough points to define the entire design space with certainty. Even when using all above mentioned methods, the design space was not defined enough, thus the found optimum points were verified and added, as well as refinement points around areas of interest. Conclusively from this study it can be seen that for more complicated scenarios, such as the optimisation of the airfoil positioning and angling, where it is difficult to visualise the design space, it is important to know how the different methods space their respective design points. For most optimisations a combination of OSF, Face-Centered CCD, and LHS should provide a sufficient baseline to define the design space well.

While the Gurney flap improved the downforce generated, it also greatly increased the drag. Depending on the need of the application, a Gurney flap would have to be weighted considering both parameters needs. A scaling of the flap would realistically only have to consider the height, as the angle made only a small impact on the generated downforce. However, as discussed previously in section 4.2, the RANS model cannot accurately predict the unsteady effects of the flap at largest flap height and angles, and therefore those results are not reliable. Thus the results can only really be trusted up until the response surface starts becoming noisy, see figure 9. Meaning the downforce the presented flap geometry provides is likely lower in reality, while the drag could also be lower. However, this would need extra investigation by using an unsteady solver or experiments.

5 Conclusions

In conclusion, optimisation is a powerful tool to maximise the performance of more complicated geometries, where the solution might not be trivial or intuitive. However, care has to be taken to ensure the design space is within reasonable bounds, in terms of mesh-, solver-, and physical-constraints. The exploration of the design space is not trivial either, and an understanding of the methods used to generate design points is important to not miss important areas of the design space. Furthermore, it is important to critically assess the optimised configurations, for example the Gurney flap which gave unreliable optimum due to the solver used.

The optimisation showed that a two airfoil setup can produce significant downforce when arranged correctly. It also showed that the addition of a Gurney flap can increase the downforce further. However, the performance is sensitive, especially to changes in the x-position when the angles are fixed in the optimised configuration. Whereas the y-position change the downforce less and barely has any influence on the drag.

References

[1] Tools A. NACA 6315 (naca6315). Retrieved from airfoiltools. com: http://airfoiltools. com/airfoil/details; 2022.

[2] Nygards E, Maligemane S. Assignment-1: Modelling and simulation of aerodynamic flows around airfoil(NACA6315).; 2021.

[3] Ismail B Celik, Urmila Ghia, Patrick J Roache, Christopher J Freitas, Hugh Coleman, Peter E Raad. Procedure for Estimation and Reporting of Uncertainty Due to Discretization in CFD Applications. ASME. 2008;130. Accessed: `http://asmedigitalcollection.asme.org/fluidsengineering/article-pdf/130/7/078001/5491455/078001_1.pdfbygueston15December2020`.

[4] ANSYS, Inc . Design Exploration User's Guide; 2013. Available at: `https://pdfcoffee.com/design-exploration-users-guide-pdf-free.html` [Accessed 2022].

[5] Ward EJK, Pinkerton R. NACA Report No. 460:" The Characteristics of 78 Related Airfoil Sections From test in the Variable-Density Wind Tunnel. Langley Aeronautical Laboratory, NACA. 1933.

[6] R Meyer, W Hage, DW Bechert, M Schatz and F Thiele. Drag Reduction on Gurney Flaps by Three-Dimensional Modifications. Journal of Aircraft. 2006;43. DOI:`10.2514/1.14294`.